Causes and Evolution of Winter Polynyas North of Greenland

Younjoo J. Lee[1], Wieslaw Maslowski[1], John J. Cassano[2,3], Jaclyn Clement Kinney[1], Anthony P. Craig[4], Samy Kamal[5], Robert Osinski[6], Mark W. Seefeldt[2,3], Julienne Stroeve[2,7], Hailong Wang[8]

[1]Naval Postgraduate School, Monterey, California, USA
[2]National Snow and Ice Data Center, Boulder, Cooperative Institute for Research in Environmental Sciences, University of Colorado, Boulder, Colorado, USA
[3]Department of Atmospheric and Oceanic Sciences, University of Colorado, Boulder, Colorado, USA
[4]Independent Researcher
[5]RedLine Performance Solutions, College Park, Maryland, USA
[6]Institute of Oceanology of the Polish Academy of Sciences, Sopot, Poland
[7]University of Manitoba, Winnipeg, Manitoba, Canada
[8]Pacific Northwest National Laboratory, Richland, Washington, USA

Correspondence to: Younjoo J. Lee (ylee1@nps.edu)

Abstract. During the 42-year period (1979-2020) of satellite measurements, four major winter (December-March) polynyas have been observed north of Greenland: one in December 1986 and the rest of them in the last decade, i.e. February of 2011, 2017 and 2018. The 2018 polynya was unparalleled by its magnitude and duration compared to the three previous events. Combined with the limited weather station and remotely-sensed sea ice data, a fully-coupled Regional Arctic System Model (RASM) hindcast simulation was utilized to examine the causality and evolution of these extreme events. We found that neither the accompanying anomalous warm surface air intrusion nor the ocean below had an impact on the development of these winter open water episodes in the study region (i.e., no significant ice melting). Instead, the extreme atmospheric wind forcing resulted in greater sea ice deformation and transport offshore, accounting for the majority of sea ice loss. Our analysis suggests that strong southerly winds (i.e., northward wind with speeds greater than 10 m/s) blowing persistently for at least 2 days or more, were required over the study region to mechanically redistribute some of the thickest sea ice out of the region and thus to create open water areas (a latent heat polynya). In order to assess the role of internal variability versus external forcing of such events, we additionally simulated and examined results from two RASM ensembles forced with output from the Community Earth System Model (CESM) Decadal Prediction Large Ensemble (DPLE) simulations. Out of 100 winters in each of the two ensembles, initialized 30 years apart, one in December 1985 and another in December 2015, respectively, 25 and 16 winter polynyas were produced north of Greenland. The frequency of polynya occurrence had no apparent sensitivity to the initial sea ice thickness in the study area pointing to internal variability of atmospheric forcing as a dominant cause of winter polynyas north of Greenland. We assert that dynamical downscaling using a high-resolution regional climate model offers a robust tool for process-level examination in space and time, synthesis with limited observations, and probabilistic forecasts of Arctic events, such as the ones being investigated here and elsewhere.

1. Introduction

The Arctic has experienced amplified warming, both through the enhancement of global temperature rise, as well as through the reductions in sea ice and snow cover that impact the regional energy budget (Serreze and Francis, 2006). This is commonly referred to as Arctic amplification (AA). On a seasonal basis, Arctic winter warming (AWW) exceeds summer warming by about a factor of four (Bintanja and van der Linden, 2013). In addition to sea ice variations, changes in the atmospheric circulation have been linked to an increase in frequency and duration of winter warming events in the Arctic (Graham et al., 2017). The trends in AWW and winter sea ice extent (SIE) have continued over the satellite record, with the March SIE decline rate of ~2.6% per decade for the period of 1979-2020, including the four lowest winter maxima of SIE in 2015-2018 and the lowest ten during 2005-2019. While SIE reductions in winter are less than ones in summer (Stroeve and Notz, 2018), there is clear supporting evidence that the winter ice pack has thinned and the amount of multi-year sea ice has declined (Kwok et al., 2009; Meier et al., 2014; Kwok, 2018; Ricker et al., 2021). It is expected that the resulting younger and thinner ice is more susceptible to atmospheric wind forcing (Spreen et al., 2011; Itkin et al., 2017), yielding increased sea ice drift speed, enhanced fracturing and more lead openings (Rampal et al., 2009). Hence, along with the current trend in the Arctic sea ice toward younger and thinner ice, it can be hypothesized that polynyas may become more prevalent in recent years. Since about half of the total atmosphere-ocean heat exchange over the Arctic Ocean may occur through leads and polynyas in winter (Maykut, 1982), the occurrence and formation of polynyas could play a crucial role in the alteration of regional climate (Morales Maqueda et al., 2004).

In late February 2018, satellite imagery revealed an unusual open water polynya north of Greenland between the Lincoln and Wandel seas (Fig. 1a). This event received considerable attention not only because it was claimed to be a one-of-a-kind extreme event involving some of the thickest Arctic sea ice but also because its emergence coincided with anomalous, above freezing, warming of surface air temperature over the region after the sudden stratospheric warming (SSW) event observed in mid-February 2018 (Moore et al., 2018). The presumed contribution of this warm surface air to the polynya opening is of interest and so are its causality, evolution and past occurrences. Yet, detailed *in situ* observations of polynyas are limited due to their intermittency and restricted access in winter. Hence, in addition to satellite measurements and weather data, fully coupled climate models become critical tools in studying such events (e.g., Ludwig et al., 2019). However, for the majority of global climate models (GCMs), many coastal polynyas are at sub-grid scales; thus, the GCM utility for comprehensive polynya studies are impeded (Weijer et al., 2017). In addition, GCMs are not intended to represent specific climate events in space and time and they are not suitable for process-level investigation of such events and quantification of their impact at both local and larger scales.

On the other hand, regional climate models (RCMs) used for dynamical downscaling are expected to show improvement in reproducing extreme weather events, given that their atmospheric boundary conditions for simulations of the past to present are derived from global atmospheric reanalysis such as Climate Forecast System (CFS) version 2 (CFSv2; Saha et al., 2011). Therefore, high-resolution RCMs, such as the Regional Arctic System Model (RASM; e.g. Maslowski et al. 2012), offer unique

capabilities for examining the spatio-temporal development and impact of observed specific events like a polynya (Fig. 1b), in the context of a fully-coupled climate system model (atmosphere-sea ice-ocean-land), while CFSv2 is shown to be less skillful in simulating such an event (Fig. 1c). In addition, RCMs afford ensemble sizes prohibitive to their global fine-resolution counterparts, which is often a requirement to distinguish the forced response from internal model variability (e.g., Peings et al. 2021).

The 2018 winter polynya north of Greenland has been investigated by Moore et al. (2018) using an ice-ocean model forced by surface atmospheric reanalysis. They have established the dominant role of surface winds in generating this polynya. Here, by taking advantage of the fully-coupled and high-resolution RASM hindcast simulation, combined with weather station and satellite sea ice data, we evaluate the capability of a RCM in reproducing the observed natural phenomena (Fig. 2) and investigate the coupled mechanisms involved in the development of northern Greenland coastal polynyas within some of the thickest Arctic ice-pack cover. In particular, this study focuses on analysis of historical winter (December-March) polynya events for the full period of satellite data availability (1979-2020) to diagnose the relative roles of thermodynamic and dynamic processes and to assess required forcing changes over the last four decades. Furthermore, by dynamic downscaling of the Community Earth System Model (CESM)-Decadal Prediction Large Ensemble (DPLE), two sets of 30 years apart RASM ensemble (termed RASM-DPLE) simulations are performed to examine the relative roles of internal variability and external forcing influencing the development of winter polynyas under two different sea ice regime scenarios: i.e. a thicker ice in the 1980s versus a thinner ice in the 2010s. We provide details of the satellite and weather station data used for this study in section 2 and the model setup for the hindcast and DPLE simulations are described in section 3. Next, section 4 presents a synthesis of observed and modeled past winter polynya results and examines the statistics of polynya occurrence and the required conditions for their generation in the RASM-DPLE simulations. This is followed by the discussion in section 5 and the study is summarized in section 6.

2 Data

2.1. Surface air temperature and wind

Hourly surface air temperature (3-hourly prior to 2015) data were obtained from the seven weather stations (World Meteorological Organization station identifier: 04221, 04254, 04285, 04351, 04330, 04312 and 04301) around Greenland (data available at https://rp5.ru) and then averaged daily for January-March of 2011, 2017, and 2018. Since wind data were incomplete at the closest weather station from the center of the polynya in 2018 (i.e., Station 04301, Cape Morris Jessup at 83° 39' N and 33° 22' W), we used 3-hourly surface wind data from the adjacent Station 04312 (Station Nord at 81°43' N and 17°47' W), which were originally binned for 16 wind directions. Also, ERA-Interim atmospheric reanalysis of 6-hourly 10 m wind fields (Dee et al., 2011; https://www.ecmwf.int/en/forecasts/datasets/reanalysis-datasets/era-interim) was used for comparison with the RASM hindcast simulation over the study region.

2.2. Sea ice concentration and thickness

Daily sea ice concentration (SIC) data were obtained via the National Snow and Ice Data Center (NSIDC): https://nsidc.org/data/G02202/versions/4 for December 1978– March 2020 (Meier et al. 2021). Satellite-derived SIC used for this study is based on passive microwave measurements using the NASA team (NT) algorithm (Cavalieri et al., 1984); all the data are on a polar stereographic 25 km×25 km grid. The daily SIC was used to examine the occurrence of a polynya in the satellite measurements. We later detected observed polynya events when the daily averaged satellite SIC dropped below 90% over the study region. RASM sea ice thickness (SIT) was also compared with the CryoSat-2/the Soil Moisture Ocean Salinity (SMOS) satellite merged data that are only available in winter months (Ricker et al., 2017) as well as CFSv2 reanalysis (https://doi.org/10.5065/D61C1TXF). Due to the lack of persistent SIT observations over the Arctic, the Pan-Arctic Ice Ocean Modeling and Assimilation System (PIOMAS) is often considered as an "observational" proxy (Zhang and Rothrock 2003; Schweiger et al. 2011; Stroeve et al. 2014). The PIOMAS (version 2.1) sea ice data were retrieved from the Polar Science Center at the University of Washington (http://psc.apl.uw.edu/research/projects/arctic-sea-ice-volume-anomaly/data/).

3 Method

3.1 Regional Arctic System Model

RASM is a limited-area, fully-coupled climate model consisting of the Weather Research and Forecasting (WRF version 3.7.1) for atmosphere, the Los Alamos National Laboratory Sea Ice Model (CICE version 5.1.2) for sea ice and Parallel Ocean Program (POP version 2.1) for ocean, the Variable Infiltration Capacity (VIC version 4.0.6) land hydrology and routing scheme (RVIC version 1.0.0) for land (see Maslowski et al. 2012; Roberts et al. 2015; DuVivier et al. 2015; Hamman et al. 2016; Hamman et al. 2017; Cassano et al. 2017). All the components are coupled using the Craig et al. (2012) version of CESM flux coupler. RASM is configured over a pan-Arctic domain, including the entire Northern Hemisphere marine cryosphere and all terrestrial drainage basins that drain to the Arctic Ocean. The ocean and sea ice components share a 1/12-degree (~9 km) rotated spherical grid and are configured with 45 levels in the vertical and five ice thickness categories, respectively. The atmosphere and land hydrology components are set up on a 50-km polar stereographic mesh with the vertical resolution of 40 levels and 3 soil layers, respectively. For the hindcast simulation (September 1979–present), CFS Reanalysis (CFSR)/CFSv2 are dynamically downscaled to provide RASM-WRF with atmospheric lateral boundary conditions and for linearly increasing grid nudging of winds and temperature for the top half of the model domain, approximately above 540 hPa. The RASM-POP ocean temperature and salinity along the closed lateral boundaries are restored to monthly Polar Science Center Hydrographic Climatology version 3.0 (PHC 3.0; Steele et al., 2001). The initial conditions at the beginning of the hindcast simulation are derived from the 32-year spin-up of the ocean-sea ice model forced with the Common Ocean-Ice Reference Experiment Inter-Annual Forcing version 2 (CORE2-IAF; Large and Yeager, 2009) atmospheric reanalysis for 1948-1979.

The RASM-DPLE simulations are derived by dynamically downscaling global atmospheric output from the initialized CESM-DPLE simulations (Yeager et al., 2018). Output from the two 10-member decadal ensembles, initialized on December 1st of 1985 and 2015, was selected for in-depth analysis under different regimes of the Arctic SIT distribution. Each RASM-DPLE simulation is initialized with the ocean and sea ice conditions, with thinner ice in the latter period (Fig. S1), from the RASM hindcast and integrated for 121 months with CESM-DPLE atmospheric forcing. The size of each ensemble (10 members) is determined by the availability of archived CESM-DPLE output necessary for RASM-WRF boundary conditions. Hence, output for 100 winters per each ensemble allows for statistical analysis of polynya occurrence in the past and near future.

3.2 Self-organizing maps

The self-organizing map (SOM), an artificial neural network based on a competitive learning algorithm (Kohonen, 2001), has been widely used to visualize input data vectors onto a low dimensional map of nodes and to objectively classify complex data sets in meteorology and oceanography (see Liu and Weisberg, 2011). For January-March 2018, the RASM/WRF pan-Arctic (>65 °N) 6-hourly surface wind fields (i.e., 10 m U and V components) are characterized using a SOM [4×4] map grid (i.e., 16 nodes or patterns). Time-dependent spatial features of near surface winds are identified and frequencies of occurrence of wind patterns favorable for a polynya are quantified using the SOM Toolbox 2.0 for MATLAB available at http://www.cis.hut.fi/projects/somtoolbox.

4 Results

4.1 2018 winter polynya – a case study

4.1.1 Near-surface air temperature around Greenland

Focusing on the most recent and the largest winter polynya event, daily near-surface air temperatures were examined from the weather stations around the Greenland coast for January-March 2018 (Fig. 3). A significant warming event (air temperatures rising above 0 ^{o}C) was observed over the northeastern Greenland region from mid-February to early March and captured well in the RASM simulation. This anomalous warming was most prominent along the northern Greenland coast (Figs. 3e and 3f), where the polynya was observed and simulated in RASM (Figs. 2a and 2d, respectively), but less pronounced over the mid-eastern Greenland coast (Figs. 3g and 3h). In contrast, no warming was measured in the southwestern stations for the same period (Figs. 3b-3d). This anomalous warming, with relative humidity rising above 90% (i.e., Station 04312; not shown), coincided with a strong reversal of the Arctic Oscillation (AO) index (https://www.cpc.ncep.noaa.gov/products/precip/CWlink/daily_ao_index/ao.shtml) from a positive to a strongly negative phase (Fig. 3a). Among the northeastern stations, the observed near-surface air temperature was positively correlated to the AO index (Fig. 3i). The maximum correlation coefficient (r) was time-lagged up to 11 days at the northern stations and only 3-4 days at the mid-eastern stations (Fig. 3j). Given that the anomalous warming started a few days earlier at the mid-eastern stations and

ceased a few days later at the northern stations, suggests the advection of warm air masses from the south. The prolonged warming at the northern stations could also be partly due to the release of oceanic heat from the polynya to the atmosphere.

On the other hand, near-surface air temperatures were inversely correlated with the AO index (Fig. 3i) in the southwestern Greenland region, with a shorter time-lag (one to two days) for a maximum correlation coefficient (Fig. 3j). We found that no anomalous warming was present in the southwestern Greenland region during February. In fact, near-surface air temperatures tended to gradually decrease from January through February, with the lowest temperatures observed between 22nd and 24th of February 2018 (Figs. 3b-3d). Thereafter, near-surface air temperatures rapidly increased at all southwestern stations, peaking in early March, corresponding to the strong negative AO phase, and the second warming came approximately two to three weeks later.

Overall, the RASM hindcast simulation captured remarkably well the sudden increase of near-surface air temperatures in northeastern Greenland and its gradual decrease. RASM also reproduced well the cooling in February and then the warming over southwestern Greenland, in terms of its magnitude and spatio-temporal variability (Fig. 3). One discrepancy in the RASM simulation against the weather stations data was a positive bias of near-surface air temperatures at Stations 04221 (Fig. 3b) and 04330 (Fig. 3g), possibly linked to the relatively coarse horizontal resolution of the RASM atmospheric component (i.e., 50 km), which is insufficient for resolving strong temperature gradients across the ocean/land/ice sheet boundary or the fidelity of the near surface temperature distribution over the Greenland Ice Sheet.

4.1.2 Sea ice dynamics

The sudden anomalous warming over northern Greenland with temperatures above 0 ^{o}C was an extreme phenomenon in 2018, considering that the long-term mean (2011-2020) of February surface air temperature is –27.8 ^{o}C at Station 04301 (Fig. 3e; Cape Morris Jesup). In addition, there were other years of anomalous warming (Figs. 4b and 4c), albeit less pronounced, when previous, smaller, polynya events occurred during February 2011 and 2017 (Figs. 2b and 2c, respectively). RASM's realistic representation of the polynya, as well as the magnitude and timing of anomalous warming, grants confidence to the examination of relative contribution of thermodynamic ice melt to the generation of the polynya, although the center of the simulated polynya is not exactly colocated with the observed one. Figure 5 shows the RASM thermal sea ice surface, lateral and bottom melting terms were all negligible (< 1 cm) over the study region when integrated for the whole month of February 2018. Hence, the dramatic rise of near-surface air temperatures by more than 25 ^{o}C above climatology and their persistence around the freezing point for several days (Fig. 3e), had no impact on sea ice melt, nor on the preconditioning and development of the polynya north of Greenland. In agreement with Moore et al. (2018), we corroborate that this polynya was driven by mechanical redistribution of sea ice outside of the study region (see Fig. 4a): i.e., this was a latent heat polynya. Based on RASM results, we calculate that between 15 and 25 February 2018, 192 km^3 of sea ice was dynamically transported outside the study region (Fig. 4d). During two weeks prior to the 2018 polynya event, a mean

thermodynamic ice growth over the region was 0.72 km^3/day (Fig. 4d), which is comparable to the rate in a non-polynya year such as 2019 (not shown). The peak sea ice growth of 3.1 km^3/day occurred on 26 February right after the maximum daily dynamic ice removal and the anomalous warming period. However, this large sea ice removal during the polynya formation period was not fully replenished in the region by the end of March, even with dynamic and thermodynamic processes adding 81 km^3 and 42 km^3, respectively, after 26 February. Overall, the RASM integrated thermodynamic ice growth in the study region during February 2018 was approximately 50% higher (31.2 km^3; Fig. 4d) due to the rapid ice growth during the polynya opening, compared to the ice growth during a non-polynya year (i.e., 20.8 km^3 in February 2019; not shown).

4.1.3 Atmospheric-sea ice coupling

As dynamic processes dominated the overall winter sea ice in the study region, we have analyzed the wind data from the weather station (Station 04301; Station Nord) and have found that the polynya development was associated with strong and persistent winds from the south-southeast (Fig. 4g). We further examined how the spatial near-surface wind fields evolved over the time period associated with the sea ice divergence. The SOM analysis extracted 16 patterns from the total of 360 synoptic wind fields: the 6-hourly RASM 10 m U- and V-wind components during January-March 2018. Figure 6 shows the four major wind patterns most frequently identified (more than 77% occurrence) from the pre-polynya period (5 February 2018) until closing of most of the open water areas (13 March 2018). The RASM hindcast simulation confirmed that this polynya event was predominantly associated with southerly to southeasterly winds blowing over the northern Greenland region (Fig. 6b and 6c), consistent with the ERA-Interim reanalysis of 10 m wind fields (Fig. S2). Prior to the polynya event in 2018, surface winds were mainly from the north or northwest over the region (Fig. 6a), which yielded little or no sea ice divergence (Fig. 6e). When the major wind pattern shifted to between southerly to southeasterly winds over the northern Greenland region on 15 February 2018 (Fig. 6b), sea ice started to deform and diverge significantly (Fig. 6f). Beginning on 20 February 2018, the southeasterly wind became even more prominent, with 19% stronger wind speed over the northern coast of Greenland (Fig. 6c), which increased the sea ice deformation rate further and led to the maximum polynya opening (Fig. 6g). The largest observed and modeled polynya areas were identified on 25 February 2018 (see Figs. 2a and 2d, respectively). Thereafter, within a week, the shift of wind patterns in late February (Fig. 6d) reversed the dynamic sea ice volume (SIV) tendency from net loss to gain (Fig. 4d) and subsequently reduced the deformation rate back to nearly zero by early March (Fig. 6h)

4.2 Winter polynyas during 2010s

4.2.1 February 2011 and 2017

Upon examining satellite-derived SIC over the data record between 2010 and 2020 (Figs. 7 and S3), we found that there were two additional polynya events in the same month, albeit smaller, over the northern Greenland region observed in February 2017 and 2011 (see Figs. 2b and 2c, respectively). Here, we found those polynya events when the daily mean satellite-derived SIC fell down to or below 90% over

the region (see Figs. 7a, 7g, and 7h,). As was the case of the 2018 polynya, both the previous events also coincided with anomalous warming, peaking on 12 February 2011 (Fig. 4b) and on 8 February 2017 (Fig. 4c), as measured at Station 04301 (Cape Morris Jesup). Near-surface air temperature variability was statistically correlated with the AO index (r=0.39, $p<0.01$ in 2011; r=0.45, $p<0.01$ in 2017), lagged by approximately two weeks. Those two polynyas were represented well in the RASM hindcast simulation (Figs. 2e and 2f) and thus we investigated their causality with respect to their relative SIV reductions due to dynamical processes and/or thermodynamic ice melt (Figs. 4e and 4f). The RASM results confirmed that those were latent heat polynyas dominated by the mechanical redistribution of sea ice out of the region. Their sizes were smaller compared to the 2018 polynya, with the one in 2017 even smaller than the one in 2011, which we attribute to somewhat different wind patterns such as its direction, magnitude and duration (Figs. 4i and 4h). Table 1 shows that, during the polynya periods based on the RASM simulation (defined here when ice volume tendency is less than –10 km^3/day for more than 3 days), i.e., 12-15 February 2011 and 8-10 February 2017, 55 km^3 and 42 km^3 of sea ice was dynamically removed outside the study region, respectively, which is much less compared to the ice loss of 189 km^3 during the 2018 event (16-25 February 2018). The size of a polynya was proportional to the pseudo-wind stress (i.e., wind speed squared) integrated over the polynya period (Table 1). Thus, more turbulent (latent plus sensible) heat was lost during the 2011 winter polynya (daily mean of –96.7 W/m^2 and maximum of –125 W/m^2) when its size was bigger (Table 2). In addition, referenced to the February ice growth during a non-polynya year (for example, 20.8 km^3 in February 2019; not shown), the RASM thermodynamic ice growth integrated over the month of February was elevated: 33% higher in 2011 (27.6 km^3; Fig. 4f) in the study region. Note that the daily mean turbulent heat flux in the study region was –48 W/m^2 during the 2018 winter polynya event with the maximum daily heat loss up to –182 W/m^2. However, the total daily turbulent heat loss was much larger than any other year because of the size and duration of open water areas (Table 2).

4.2.2 What is driving changes in polynya frequency

Given the above analysis, an outstanding question is why winter polynyas became more frequently observed during the 2010s within the past four decades. Since observational data around northern Greenland are incomplete, we expanded the analysis of surface wind fields (10 m U and V components) from the RASM hindcast simulation near Station 04312 (Fig. 8a; Station Nord) and Station 04301 (Fig. 8b; Cape Morris Jesup). Our analysis revealed that northward wind (blowing from south), required for opening of a winter polynya along the coast of northern Greenland, has recently become more frequent, stronger (i.e., wind speed >10 m/s), and more persistent (i.e., blowing for at least 2 consecutive days or longer). In addition, the three years of winter polynya occurrence with the wind conditions satisfied the above criteria. Based on the RASM hindcast simulation, the grid mean wind conditions in February 2009 were similar to the ones in February 2017 near Station 04312 (Fig. 8a), but a notable polynya was not detected, possibly owing to the influence by such wind conditions over a smaller area within the main polynya region. The observational data also indicate a polynya favorable wind condition in 2009: i.e., relatively warmer air (–12.6 °C) blowing from the south-southwest with the maximum wind speed of 19 m/s on February 7th, 2009 at Station 04312 (Table S1). But, the satellite-derived mean daily SIC only dropped down to 94% in February 2009 (Fig. S4o) because the wind was possibly weaker,

compared to the wind condition in February 2017 (Fig. 4i). Note that the early February 2009 data at Station 04312 are missing and the entire February 2009 data at Station 04301 are completely unavailable. Althouh changes in wind (i.e., direction and intensity) play a role in this region, we cannot completely rule out that a thinning of sea ice may promote more frequent polynyas in recent years. Hence, we additionally simulated two large ensembles and evaluated model representation of polynyas in section 4.4.

4.3 Winter polynyas between 1980s and 2000s

It is interesting to point out that no major winter polynya was found during the 1980s to 2000s (Figs. S3 and S4) except one major event in December 1986; the lowest daily mean SIC was 82% over the study region on 15 December 1986 (Fig. S4i). There were two instances indicating possible polynya events because the regional daily mean SIC was below 90%, i.e. , December 1984-January 1985 (Fig. S4g) and December 2002-January 2003 (Fig. S3i). However, they were not considered polynyas in this study since sea ice dynamic volume tendency (DVT) was not below the threshold (≤ -10 km^3/day) for at least three consecutive days (Fig. S5). Compared to the recent polynyas in the 2010s, the polynya in December 1986 is larger than ones in 2011 and 2017 but smaller than one in 2018. The satellite SIC shows that the polynya occurred in a similar location to the ones in the 2010s (Fig. 9a) and the RASM simulation also captured it well (Fig. 9b). The RASM simuation confirms that the December 1986 event was not associated with significant ice melting (Fig. 9c) although it was slightly elevated, compard to the 2018 event (Fig. 5). Analogous to the recent 2010s polynyas, the December 1986 polynya is linked to a strong southerly wind of almost the same strength as the 2018 winter polynya (Fig. 9d and Table 2), but its duration was shorter (the strong southerly wind only lasted 5 days; Fig. S6). Other features in common are that anomalous atmospheric warming occurred during the polynya and that the near-surface air temperature was positively correlated (r=0.45, $p<0.05$) to the AO index (Fig. 9e). The correlation was lagged by 11 days, similar to the event in February 2018. However, no SSW was reported during winter 1986-1987 (see Butler et al., 2017) and it was an El Niño winter in contrast to the polynyas of the 2010s. The RASM hindcast simulation suggests that, between 12 and 16 December 1986, 142 km^3 of sea ice was dynamically transported outside the study region (Fig. 9f), which is 25% less than the amount of ice removed in 2018, and this was 2.6 times more than the ice transported in February 2011 (Table 1). However, the mean turbulent heat flux was much less in December 1986 than in February 2011 even though it was a larger event in terms of polynya size and wind intensity. This is possibly due to the fact that sea ice was thicker in 1986; for example, the mean SIT was 4.4 m for 5 days before the polynya (Table 1). Due to large open water areas in December 1986, the integrated turbulent heat loss was much larger compared to the polynyas in February 2011 and 2017.

4.4 Polynyas in a large ensemble of initialized decadal prediction simulations

According to the merged CryoSat-2/SMOS data, the mean SIT over the region does not exhibit a negative trend in February. For example, in the first week of February, the mean SIT was 2.74 m in 2011, 3.16 m in 2017, and 2.73 m in 2018. On the other hand, the RASM hindcast simulation indicates

a gradual thinning of sea ice in the region and a long-term trend of SIT was –0.26 m/decade for all months during 1985-2019 (not shown). In order to further investigate the potential role of regional sea ice thickness reduction versus internal variability in the occurrence of winter polynya events north of Greenland, we performed and examined two RASM 10-member ensembles forced with atmospheric output from the CESM-DPLE simulations. They are initialized 30 years apart, i.e. in December 1985 and 2015, respectively, to represent different SIT conditions over the study region, with the former corresponding to a thicker ice regime (Fig. S1a; mean SIT of 3.3 m) and the latter to a thinner ice regime (Fig. S1b; mean SIT of 2.3 m). Note that the PIOMASS SIT also corroborates that sea ice was 1.1 m thicker north of Greenland in November 1985 (Fig. S1d; mean SIT of 3.3 m) than in November 2015 (Fig. S1e; mean SIT of 2.2 m). Each ensemble member is integrated forward for 10 years, thus resulting in 100 winters (i.e., 10 ensemble members for each 10-year simulation) for statistical analysis of polynya occurrence in each of the two ensembles. Note that because of the setup of these experiments (i.e. using the CESM DPLE atmospheric output as boundary conditions for forcing the RASM-DPLE fully-coupled simulations), we only compared the probability of polynya occurrence during winter months (December-March) instead of focusing on accurate temporal representation of such events in a similar location.

Taking as the baseline the winter polynya in February 2017 (Fig. 4e and Table 1), which was the smallest among the three observed events, we defined "a latent heat polynya" in the RASM-DPLE ensemble members when a daily winter sea ice loss due to dynamic processes was greater than 10 km^3/day for at least three consecutive days over the study area (see Fig. 4a). Note that the three other observed polynya events experienced 4, 5 and 10 consecutive days of dynamic sea ice loss greater than 10 km^3/day during February 2011 (Fig. 4f), December 1986 (Fig. 9f) and February 2018 (Fig. 4d), respectively (Table 1). Analogous to the RASM hindcast simulation, Tables 3 and 4 list all the polynya occurrences from the two ensemble runs. We found 25 polynyas in the 1985-initialized ensemble (Table 3) and 16 polynyas in the 2015-initalized ensemble (Table 4), out of the 100 winters each. Note that some ensemble members simulate more than 1 polynya event while some had no polynyas at all. The majority of the polynya events (84% in the 1985-initialized and 69% in the 2015-initialized runs) were similar in size to the smaller polynyas that were simulated in February of 2011 or 2017. The longer-lasting polynyas (with dynamic sea ice removal $\geq$ 10 km^3/day for five consecutive days or longer) were also produced in the RASM-DPLE simulations: four incidents in the 1985-initialized and five incidents in the 2015-initialized runs.

We finish this analysis of RASM-DPLE results by comparing the longest polynya detected in each ensemble (see Table 3 and 4), i.e., from the ensemble member #4 in January 1988 (Fig. 10a) and the ensemble member #2 in January 2024 (Fig. 10b). As in the case of observed events, these latent heat polynyas were created due to dynamic sea ice transport (DVT $\leq$ –10 km^3/day for seven consecutive days), resulting in significant sea ice removal of –120 km^3 out of the region in 1988 (Fig. 10c; Table 3) and –136 km^3 in 2024 (Fig. 10d; Table 4). By cross-examining wind patterns over northern Greenland (i.e., near Cape Morris Jesup), our analysis confirmed that these large polynya openings were also associated with very strong and persistent southerly winds in the RASM-DPLE simulations (Figs. 10e and 10f). We found that daily DVT and meridional wind were significantly correlated, and the size of

polynyas was highly dependent on the pseudo-wind stress integrated over the polynya period (Table 3 and 4). However, given the wind patterns, their duration and the integrated sea ice removal (–189 km^3) during the observed polynya in February 2018 (Table 1), this event stands out within all the RASM results analyzed in this study. Compared to the 2018 event, the slight difference in the magnitudes between the largest polynyas of each ensemble still does not imply much significance of SIT in their generation and evolution. Overall, the more frequent winter polynyas, produced in a thicker sea ice regime between the two 30-year apart ensembles, implies that changes in SIT are not significant contributors (at least up to now) to the generation of such events for this region during wintertime. Therefore, the findings support that polynyas becomes prevalent when southerly winds are more persistent and stronger in northern Greenland.

5 Discussion

The recent studies (i.e., Moore et al., 2018; Ludwig et al., 2019) used an ice-ocean model to study the polynya in February 2018, which means that the model is prescribed with reanalysis or gridded products on every grid cell. On the other hand, RASM is a fully-coupled high resolution regional model, which allows us to further study interactions between ice, ocean, and atmosphere. When RASM is used for dynamical downscaling, atmospheric forcing is prescribed only along the lateral boundaries and nudged above approximately 500 hPa. Hence, surface atmospheric forcing is predicted every coupling time step. Although the RASM near surface wind fields agree well with the reanalysis data, it is possible that a slight discrepancy in wind direction or magnitude near the study region may have shifted the center of the polynya more westward than was observed. Although the RASM hindcast simulation relies on the CFSv2 atmospheric conditions, the winter SIT on February 25th, 2018 is very unrealistic in CFSv2 with too thick ice in the central Arctic. This is a common bias in current climate models (i.e., Watts et al., 2021), resulting from limitations in or lack of representation of key physical processes, partly due to their coarse model resolution (e.g., Chassignet et al., 2020). Since the CFSv2 wind and temperature are used only above approximately 500 hPa, the dynamic downscaling approach using the high-resolution fully-coupled RASM allows resolving the fine-scale processes and provides valuable insight into the mechanism of the generation and evolution of winter polynyas off the northern coast of Greenland. We examined the occurrence of such events in RASM against the satellite observations in winter months (December-March) over the past four decades (1979-2020). The results from the RASM hindcast simulation suggest that the size of a winter latent heat polynya in this region is sensitive to the direction, magnitude and duration of near-surface winds.

Subject to the limited sample sizes, we find that the generation of a winter polynya in this region requires strong southerly winds (i.e., speeds >10 m/s and lasting for more than 2 days largely over the study region based on the RASM hindcast simulation). Table 1 and Figure 8 show that the stronger and more persistent the southerly wind blows, the larger the winter polynya becomes regardless of ice conditions in the study region, but it is not immediately clear what causes such changes in wind patterns. At the same time, it is reported that the southerly winds might reduce sea ice export through Fram Strait by a slowdown of sea ice drift (Wang et al., 2021). The RASM simulation captures such

decline in 2018 and overall agrees with the observed interannual variability of ice export through the Fram Strait (Fig. S7; see also Smesdrud et al., 2017), indicating that atmospheric wind variability is well represented over the region. However, apart from the polynya region, sea ice coverage is overestimated especially north of Svalvard (Fig. 1b) where basal melting plays a role (Fig. 5c). This may suggest that ocean heat delivered via the West Spitsbergen Current is not strong enough to melt sea ice along its path into the Arctic. It can also be speculated that this region might have been affected by increasing extreme winter storm activities in recent years that are associated with anomalous warming events. However, no significant trends were found in January-February during 1979-2015 (Rinke et al., 2017).

Considering the overall vulnerability and fate of some of the thickest sea ice in the Arctic under the recent warming climate, sea ice may become susceptible to modulation by the atmospheric forcing. Sensitivity experiments indicate that a polynya would occur under the same atmospheric conditions of February 2018 even in the thick ice conditions like the winter of 1979 (Moore et al., 2018). By taking advantage of an ensemble approach, the internal variability is better assessed with respect to the occurrence of such coastal polynyas during extereme events. The RASM-DPLE study shows that the frequency, size and duration of winter polynyas is unaffected by sea ice thinning, showing no apparent difference in polynya size or frequency of occurance over time between the two ensembles initialized with two different sea ice regimes 30 years apart: 1980s vs 2010s. One interesting feature is that winter polynyas mostly (16 out of 25) occur in December-January in the 1985-initialized simulations whereas they are more prevalent (12 out of 16) in January-February in the 2015-initalized ensemble runs. In addition, the range of 5-day mean SIT before the occurrence of each polynya was 2.9-4.4 m (with a mean of 3.7 m and standard deviation of 0.36 m) in the 1985-initialized RASM-DPLE ensemble and 1.8-3.4 m (with a mean of 2.8 m and standard deviation of 0.36 m) in the 2015-initialized RASM-DPLE ensemble (Table 3 and 4, respectively). Although sea ice is thicker, the 1985-initialized ensemble simulations produce 56% more polynyas than the 2015-initialized ones. Hence, regardless of the SIT decline over the region, this study suggests that the primary necessary condition for a winter polynya occurrence is strong and persistent southerly winds. With the maximum wind speed exceeding 20 m/s and duration for 10 days, the 2018 winter polynya remains unique by any of these metrics.

When the polynyas occurred over the region, they coincided with a reversal (from the positive to negative) of the daily AO index. For instance, during the 2017-2018 winter, the AO shifted significantly from a positive phase to a strong negative phase between mid-February to early March (Fig. 3a), which was associated with weakening of the polar vortex and allowed warmer air into the Arctic. Alternatively, Kim et al. (2014) argued that due to sea ice loss especially in the Barents-Kara seas, the weakened stratospheric polar vortex preferentially induced a negative phase of the AO at the surface, resulting in warm air moving into the Arctic. This anomalous warming event occurred coincidently after the SSW event observed in mid-February 2018 (Moore et al., 2018; Rao et al. 2018), which developed into a vortex split (Lü et al., 2020). Subsequently, the winter weather was severe with intense cold air across Europe in March 2018 (Overland et al., 2020). Although the exact cause of SSW variability in still under debate, SSWs are generally known to cause anomalous warming over Greenland and impact surface weather patterns down to mid-latitudes (Butler et al., 2017). The frequency of their occurrence

is enhanced by El Niño conditions (Polvani et al., 2017) and may also be enhanced during La Niña winters depending on SSW definitions (Song and Son, 2018). For example, La Niña was in winter 2017-2018, while El Niño was in December 1986. In the recent winters with SSW (Butler et al., 2017; Rao et al., 2018; Knight et al., 2021), no winter polynya events occurred except in February 2018. In other words, the winter polynyas in 1986, 2011, and 2017 were not associated with SSW.

The opening of polynyas in the region between the Wandel and Lincoln seas primarily depends on a large-scale surface pressure pattern change, resulting in strengthening of intense southerly winds that are short-lived and sporadic. Toward the end of each polynya event, the rate of thermodynamic ice growth generally increased (Figs. 4d, 4e and 4f). The maximum rate of ice growth happened not when sea ice removal was largest with strong southerly wind but when air temperature started to significantly drop (Fig. 4). Upward surface turbulent heat fluxes continued even after DVT became positive (i.e., Table 2 and Fig. 4) when wind direction was reversed (i.e., Fig. 6d) until the open water area was completely covered by ice. In general, the rate of new ice formation in winter is expected to be high during an open water phase, such as leads and polynyas, due to an intense turbulent heat (sensible and latent) loss to the atmosphere. In some polynya regions, turbulent heat loss is as high as 300 W/m^2 such as along the Weddell Sea coast (see Morales Maqueda el a., 2004). However, the mean daily turbulent heat loss in the study region was about 61 W/m^2 in 2018 (with the daily maximum of 124 W/m^2), which is similar to the model estimates; the average/maximum daily heat fluxes from the ocean to the atmosphere are 40 and 124 W/m^2, respectively (Ludwig et al., 2019). Those values are much smaller than that in the St. Lawrence Island polynya (412 W/m^2; Pease, 1987) and Okhotsk Sea coast (471 W/m^2; Alfultis and Martin, 1987), but comparable to the Northeast Water (NEW) polynya (31 W/m^2; Morales Maqueda el al., 2004). Nevertheless, new sea ice formation was somewhat slowed down in the study region because the air-sea temperature difference was much smaller than in the other regions listed above due to the anomalously warm air carried by southerly winds over northern Greenland.

RASM estimated a maximum polynya size of 13,000 km^2, where SIT is less than 10 cm, on that day while Ludwig et al. (2019) calculated it as large as approximately 60,000 km^2 using satellite SIC, although there are large uncertainties between different satellite algorithms. For example, MODIS SIC underestimates open water areas by about 50%, compared to the Advanced Microwave Scanning Radiometer 2 (AMSR2) SIC (see Fig. 3 in Ludwig et al. (2019)). On the other hand, the RASM polynya size is based on SIT and its maximum size could increase to 29,400 km^2 if a threshold of SIT less than 25 cm is applied. According to the RASM simulation between February 1st to March 31st, 2018, the study region lost approximately 208 km^3 of sea ice due to mechanical ice removal. Although sea ice was added later by the dynamic replenishment (102 km^3) and the thermodynamic ice growth (64 km^3), the deficit of SIV was about 42 km^3, which is equivalent to the 36 cm reduction of mean SIT over the study region. However, von Albedyll et al. (2021) showed that that the thermodynamic and dynamic processes were almost equally contributed to the mean SIT change between February 25th and March 31st, 2018. Ludwig et al. (2019) calculated the ice volume thermodynamically produced (33 km^3) including the polynya period (February 14th to March 31st, 2018) using the freezing degree day parameterization, but RASM produced slightly more sea ice for the same period (53 km^3). Although an ice cover was re-established with a mean thickness of 1.96 m at the end of March 2018 (von Albedyll et

al., 2021), sea ice in the northern Greenland region was not fully restored even a month after the peak ice removal on February 25th, 2018 unlike the events in 2011 and 2017 (Fig. 4d). The CryoSat-2/SMOS data also confirmed the similar sea ice loss in the region; at the end of March 2018, the mean sea ice north of Greenland was relatively thinner (2.45 m), compared to the beginning of February (2.73 m). Therefore, one could hypothesize that the 2018 winter polynya event could have contributed to the preconditioning of the polynya event in the following summer (Schweiger et al., 2021), which was observed at a similar location. Hence the winter event might have been unprecedented by yet another measure, as polynya events have never repeated within a year over the study region except during 2018.

6 Summary

Following the previous studies of the 2018 winter polynya by Moore et al. (2018) and Ludwig et al. (2019), this study demonstrates that an additional three observed winter open water events occurred under a specific wind pattern, which removes sea ice mechanically out of the region:, i.e., December 1986 as well as February 2011 and 2017. In all of the events, the wind direction was primarily from the south and southwest (Figs. 4i and 4h). The size of polynya depended on the strength and persistence of southerly winds, and the polynya closure was a result of the relaxation of these conditions. Although the atmospheric conditions were associated with SSW in February 2018, other winter polynyas occurred in non-SSW winters. Rather, they coincided with a reversal of the AO from a positive to a negative phase. The polynya was larger in February 2011 compared to the one in 2017 because wind duration was longer: 4 days of strong southerly wind (> 10 m/s) in 2011 compared to 2 days in 2017 (Fig. 8a). Hence, 31% more sea ice was removed in the former, although wind speed and wind stress were similar between the two years (Table 1). The observed polynya in February 2018 was the largest one over the satellite SIC record since 1979. It resulted from much stronger and more persistent southerly-southeasterly winds (Fig. 4g) off the coast of northern Greenland, the direction which could also be more favorable for polynya opening (Kawaguchi et al., 2010). Although southerly wind in December 1986 was as strong as in February 2018, its duration was shorter and thus not only the size of the polynya, but also the turbulent heat flux, was relatively smaller. Sea ice was significantly thicker in the 1980s in north of Greenland, but more polynyas were not prevalent with thinner ice in the winters of 2015-2025 from the two RASM-DPLE ensembles. Given the more frequent rate of winter polynya occurrence and their apparent lack of sensitivity to the initial sea ice thickness, we conclude that a dominant cause of these winter polynyas stems from internal variability of atmospheric forcing rather than from the forced response to a warming climate.

Acknowledgement

This work was funded by NSF OPP IAA1603602 (NPS), DOE RGMA DE-SC0014117 (NPS), NSF OPP-1603544 (CU Boulder), the Canada 150 Chair program (J. S.), and the Ministry of Science and Higher Education in Poland (R. O.) in the frame of international project agreement 3808/FAO/2017/0. The PNNL is operated for the U.S. DOE by Battelle Memorial Institute under contract DE-AC05-76RL01830. In addition, computing resources were provided by the U.S. DOD High Performance

Computer Modernization Program (HPCMP). The merging of CryoSat-2 und SMOS data was funded by the ESA project SMOS & CryoSat-2 Sea Ice Data Product Processing and Dissemination Service and data from February 2011 to 2018 were obtained from https://www.meereisportal.de (grant: REKLIM-2013-04). We thank the reviewers for providing helpful comments, which improved an earlier version of this publication.

Competing interestsCode/data availability

All RASM simulations are archived in the HPCMP archive system and will be available upon publication according to the U.S. DOD data policy.

Competing interests

The authors declare no competing interests.

Author contributions

Y. L. and W. M. conceived the study and wrote the paper. A. C., S. K., R. O., and M. S. undertook the implementation and development of the RASM simulation. J. C., J. C. K., J. S., and H. W. contributed to the interpretation of results. All authors except S. K. and A. C. commented on the manuscript.

References

Alfultis, M. A., & Martin, S. (1987). Satellite passive microwave studies of the Sea of Okhotsk ice cover and its relation to oceanic processes, 1978–1982. *Journal of Geophysical Research: Oceans*, 92(C12), 13013-13028.

Bintanja, R., & Van der Linden, E. C. (2013). The changing seasonal climate in the Arctic. *Scientific reports*, *3*(1), 1-8.

Butler, A. H., Sjoberg, J. P., Seidel, D. J., & Rosenlof, K. H. (2017). A sudden stratospheric warming compendium. *Earth Syst. Sci. Data*, *9*, 63–76. https://doi.org/10.5194/essd-9-63-2017

Cassano, J. J., DuVivier, A., Roberts, A., Hughes, M., Seefeldt, M., Brunke, M., et al. (2017). Development of the Regional Arctic System Model (RASM): near-surface atmospheric climate sensitivity. *Journal of Climate*, *30*(15), 5729-5753.

Cavalieri, D. J., Gloersen, P., & Campbell, W. J. (1984). Determination of sea ice parameters with the Nimbus 7 SMMR. *Journal of Geophysical Research: Atmospheres*, *89*(D4), 5355-5369.

Chassignet, E. P., Yeager, S. G., Fox-Kemper, B., Bozec, A., Castruccio, F., Danabasoglu, G., ... & Xu, X. (2020). Impact of horizontal resolution on global ocean–sea ice model simulations based on the experimental protocols of the Ocean Model Intercomparison Project phase 2 (OMIP-2). *Geoscientific Model Development*, 13(9), 4595-4637.

Craig, A. P., Vertenstein, M., & Jacob, R. (2012). A new flexible coupler for earth system modeling developed for CCSM4 and CESM1. *The International Journal of High Performance Computing Applications*, 26(1), 31-42.

Dee, D. P., Uppala, S. M., Simmons, A. J., Berrisford, P., Poli, P., Kobayashi, S., et al. (2011). The ERA-Interim reanalysis: Configuration and performance of the data assimilation system. *Quarterly Journal of the royal meteorological society*, 137(656), 553-597.

DuVivier, A. K., Cassano, J. J., Craig, A., Hamman, J., Maslowski, W., Nijssen, B., et al. (2016). Winter atmospheric buoyancy forcing and oceanic response during strong wind events around southeastern Greenland in the Regional Arctic System Model (RASM) for 1990–2010. *Journal of Climate*, *29*(3), 975-994.

Graham, R. M., Cohen, L., Petty, A. A., Boisvert, L. N., Rinke, A., Hudson, S. R., et al. (2017). Increasing frequency and duration of Arctic winter warming events. *Geophysical Research Letters*, *44*(13), 6974–6983. https://doi.org/10.1002/2017GL073395.

Hamman, J., Nijssen, B., Brunke, M., Cassano, J., Craig, A., DuVivier, A., et al. (2016). Land surface climate in the regional Arctic system model. *Journal of Climate*, *29*(18), 6543-6562.

Hamman, J., Nijssen, B., Roberts, A., Craig, A., Maslowski, W., & Osinski, R. (2017). The coastal streamflow flux in the Regional Arctic System Model. *Journal of Geophysical Research: Oceans*, *122*(3), 1683-1701.

Itkin, P., Spreen, G., Cheng, B., Doble, M., Girard-Ardhuin, F., Haapala, J., et al. (2017). Thin ice and storms: Sea ice deformation from buoy arrays deployed during N-ICE2015. *Journal of Geophysical Research: Oceans*, *122*(6), 4661-4674.

Kawaguchi, Y., Nihashi, S., Mitsudera, H., & Ohshima, K. I. (2010). Formation mechanism of huge coastal polynyas and its application to Okhotsk northwestern polynya. *Journal of physical oceanography*, *40*(11), 2451-2465.

Kim, B. M., Son, S. W., Min, S. K., Jeong, J. H., Kim, S. J., Zhang, X., ... & Yoon, J. H. (2014). Weakening of the stratospheric polar vortex by Arctic sea-ice loss. *Nature communications*, 5(1), 1-8.

Knight, J., Scaife, A., Bett, P. E., Collier, T., Dunstone, N., Gordon, M., ... & Walker, B. (2021). Predictability of European Winters 2017/2018 and 2018/2019: Contrasting influences from the Tropics and stratosphere. A*tmospheric Science Letters*, 22(1), e1009.

Kohonen, T. (2001). Self-Organizing Maps, third ed. Springer-Verlag, New York.

Kwok, R. (2018). Arctic sea ice thickness, volume, and multiyear ice coverage: losses and coupled variability (1958–2018). *Environmental Research Letters*, *13*(10), 105005. https://doi.org/10.1088/1748-9326/aae3ec.

Kwok, R., Cunningham, G. F., Wensnahan, M., Rigor, I., Zwally, H. J., & Yi, D. (2009). Thinning and volume loss of the Arctic Ocean sea ice cover: 2003–2008. *Journal of Geophysical Research*, *114*(C7), C07005. https://doi.org/10.1029/2009JC005312.

Large, W., & Yeager, S. G. (2009). The global climatology of an interannually varying air–sea flux data set. *Climate dynamics*, 33(2-3), 341-364.

Liu, Y., & Weisberg, R. H. (2011). A review of Self-Organizing Map applications in meteorology and oceanography. In Self-Organizing Maps - Applications and Novel Algorithm Design, Edited by J. I. Mwasiagi, InTech, Rijeka, Croatia, ISBN 978-953-307-546-4, pp.253-272.

Lü, Z., Li, F., Orsolini, Y. J., Gao, Y., & He, S. (2020). Understanding of European cold extremes, sudden stratospheric warming, and Siberian snow accumulation in the winter of 2017/18. *Journal of Climate*, 33(2), 527-545.

Ludwig, V., Spreen, G., Haas, C., Istomina, L., Kauker, F., & Murashkin, D. (2019). The 2018 North Greenland polynya observed by a newly introduced merged optical and passive microwave sea-ice concentration dataset. *Cryosphere*, *13*(7).

Maslowski, W., Kinney, J. C., Higgins, M., & Roberts, A. (2012). The future of Arctic sea ice. *Annual Review of Earth and Planetary Sciences*, *40*.

Maykut, G. A. (1982). Large-scale heat exchange and ice production in the central Arctic. *Journal of Geophysical Research*, *87*(C10), 7971. https://doi.org/10.1029/JC087iC10p07971.

Meier, W. N., Fetterer, F., Windnagel, A. K., & Stewart., J. S. (2021). NOAA/NSIDC Climate Data Record of Passive Microwave Sea Ice Concentration, Version 4. Boulder, Colorado USA. NSIDC: National Snow and Ice Data Center. doi: https://doi.org/10.7265/efmz-2t65.

Meier, W. N., Hovelsrud, G. K., van Oort, B. E. H., Key, J. R., Kovacs, K. M., Michel, C., et al. (2014). Arctic sea ice in transformation: A review of recent observed changes and impacts on biology and human activity. *Reviews of Geophysics*, *52*(3), 185–217. https://doi.org/10.1002/2013RG000431.

Moore, G. W. K., Schweiger, A., Zhang, J., & Steele, M. (2018). What Caused the Remarkable February 2018 North Greenland Polynya? *Geophysical Research Letters*. https://doi.org/10.1029/2018GL080902.

Morales Maqueda, M. A., Willmott, A. J., & Biggs, N. R. T. (2004). Polynya Dynamics: a Review of Observations and Modeling. *Reviews of Geophysics*, *42*(1), RG1004. https://doi.org/10.1029/2002RG000116.

Overland, J., Hall, R., Hanna, E., Karpechko, A., Vihma, T., Wang, M., & Zhang, X. (2020). The polar vortex and extreme weather: the Beast from the East in winter 2018. *Atmosphere*, 11(6), 664.

Pease, C. H. (1987). The size of wind-driven coastal polynyas. *Journal of Geophysical Research: Oceans*, 92(C7), 7049-7059.

Peings, Y., Labe, Z. M., & Magnusdottir, G. (2021). Are 100 ensemble members enough to capture the remote atmospheric response to +2° C Arctic sea ice loss? Journal of Climate, 34(10), 3751-3769.

Polvani, L. M., Sun, L., Butler, A. H., Richter, J. H., & Deser, C. (2017). Distinguishing stratospheric sudden warmings from ENSO as key drivers of wintertime climate variability over the North Atlantic and Eurasia. *Journal of Climate*, 30(6), 1959-1969.

Rampal, P., Weiss, J., Marsan, D., & Bourgoin, M. (2009). Arctic sea ice velocity field: General circulation and turbulent-like fluctuations. *Journal of Geophysical Research*, *114*(C10), C10014. https://doi.org/10.1029/2008JC005227.

Rao, J., Ren, R., Chen, H., Yu, Y., & Zhou, Y. (2018). The stratospheric sudden warming event in February 2018 and its prediction by a climate system model. *Journal of Geophysical Research: Atmospheres*, *123*(23), 13-332.

Ricker, R., Kauker, F., Schweiger, A., Hendricks, S., Zhang, J., & Paul, S. (2021). Evidence for an increasing role of ocean heat in Arctic winter sea ice growth. *Journal of Climate*, 34(13), 5215-5227.

Ricker, R., Hendricks, S., Kaleschke, L., Tian-Kunze, X., King, J., & Haas, C. (2017). A weekly Arctic sea-ice thickness data record from merged CryoSat-2 and SMOS satellite data. *The Cryosphere*, 11(4), 1607-1623.

Rinke, A., Maturilli, M., Graham, R. M., Matthes, H., Handorf, D., Cohen, L., et al. (2017). Extreme cyclone events in the Arctic: Wintertime variability and trends. *Environmental Research Letters*, *12*(9), 094006.

Roberts, A., Craig, A., Maslowski, W., Osinski, R., DuVivier, A., Hughes, M., et al. (2015). Simulating transient ice-ocean Ekman transport in the Regional Arctic System Model and Community Earth System Model. *Annals of glaciology*, *56*(69), 211-228.

Saha, S., Moorthi, S., Wu, X., Wang, J., Nadiga, S., Tripp, P., et al. (2011). NCEP Climate Forecast System Version 2 (CFSv2) 6-hourly Products. Research Data Archive at the National Center for Atmospheric Research, Computational and Information Systems Laboratory. https://doi.org/10.5065/D61C1TXF.

Schweiger, A. J., Steele, M., Zhang, J., Moore, G. W. K., & Laidre, K. L. (2021). Accelerated sea ice loss in the Wandel Sea points to a change in the Arctic's Last Ice Area. Communications Earth & Environment, 2(1), 1-11.

Schweiger, A., Lindsay, R., Zhang, J., Steele, M., Stern, H., & Kwok, R. (2011). Uncertainty in modeled Arctic sea ice volume. *Journal of Geophysical Research: Oceans*, 116(C8).

Serreze, M. C., & Francis, J. A. (2006). The Arctic amplification debate. *Climatic change*, *76*(3-4), 241-264.

Song, K., & Son, S. W. (2018). Revisiting the ENSO–SSW relationship. *Journal of Climate*, 31(6), 2133-2143.

Spreen, G., Kwok, R., & Menemenlis, D. (2011). Trends in Arctic sea ice drift and role of wind forcing: 1992-2009. *Geophysical Research Letters*, *38*(19). https://doi.org/10.1029/2011GL048970.

Steele, M., Morley, R., & Ermold, W. (2001). PHC: A global ocean hydrography with a high-quality Arctic Ocean. *Journal of Climate*, 14(9), 2079-2087.

Stroeve, J., & Notz, D. (2018). Changing state of Arctic sea ice across all seasons. Environmental Research Letters, 13(10), 103001.

Stroeve, J., Barrett, A., Serreze, M., & Schweiger, A. (2014). Using records from submarine, aircraft and satellites to evaluate climate model simulations of Arctic sea ice thickness. *The Cryosphere*, 8(5), 1839-1854.

von Albedyll, L., Haas, C., & Dierking, W. (2021). Linking sea ice deformation to ice thickness redistribution using high-resolution satellite and airborne observations. *The Cryosphere*, 15(5), 2167-2186.

Wang, Q., Ricker, R., & Mu, L. (2021). Arctic sea ice decline preconditions events of anomalously low sea ice volume export through Fram Strait in the early 21st century. Journal of Geophysical Research: Oceans, 126(2), e2020JC016607.

Watts, M., Maslowski, W., Lee, Y. J., Kinney, J. C., & Osinski, R. (2021). A spatial evaluation of Arctic sea ice and regional limitations in CMIP6 historical simulations. *Journal of Climate*, 34(15), 6399-6420.

Weijer, W., Veneziani, M., Stössel, A., Hecht, M. W., Jeffery, N., Jonko, A., et al. (2017). Local Atmospheric Response to an Open-Ocean Polynya in a High-Resolution Climate Model. *Journal of Climate*, *30*(5), 1629–1641. https://doi.org/10.1175/JCLI-D-16-0120.1.

Yeager, S.G., Danabasoglu, G., Rosenbloom, N.A., Strand, W., Bates, S.C., Meehl, G.A., Karspeck, A.R., Lindsay, K., Long, M.C., Teng, H. and Lovenduski, N.S., 2018. Predicting near-term changes in the Earth System: A large ensemble of initialized decadal prediction simulations using the Community Earth System Model. *Bulletin of the American Meteorological Society*, 99(9), pp.1867-1886.

Zhang, J., & Rothrock, D. A. (2003). Modeling global sea ice with a thickness and enthalpy distribution model in generalized curvilinear coordinates. *Monthly Weather Review*, 131(5), 845-861.

Table 1. Characteristics of the polynya events, when daily dynamic sea ice removal is greater than 10 km^3/day (i.e., dynamic volume tendency (DVT) ≤ –10 km^3/day) for more than three consecutive days, and the corresponding wind condition near a weather station, as well as sea ice thickness (SIT) over northern Greenland from the RASM hindcast simulation (1980-2020).

Year	Date when DVT ≤ –10 km^3/day (No. of polynya days)	Five-day mean SIT (m) before polynya	Daily Mean DVT (km^3/day)	Total sea ice removal (km^3)	North-South wind during polynya			Nearest weather station
					Time-integrated Pseudo–wind stress* ($m^2/s^2 \cdot day$)	Mean speed (m/s)	Max. speed (m/s)	
1986	12-16 Dec (5 days)	4.4	–28.4	–142	717	11.0	17.6	Cape Morris Jessup
2011	12-15 Feb (4 days)	3.6	–13.8	–55	476	10.2	15.1	Station Nord
2017	8-10 Feb (3 days)	3.3	–14.0	–42	354	9.5	15.3	Station Nord
2018	16–25 Feb (10 days)	3.2	–18.9	–189	1486	11.3	21.8	Cape Morris Jessup

*only for the northward wind component

Table 2. Daily mean net turbulent (sensible and latent) heat flux (W/m^2) and its standard deviation (s.d.) during the polynya events over open water areas (km^2), where sea ice thickness (SIT) is less than 10 cm, from the RASM hindcast and DPLE simulations. The negative values indicate heat loss from the polynya to the atmosphere.

RASM Cases		Year	Date	Daily Turbulent Flux (W/m^2)			Daily Open Water Area (km^2)			Total integrated turbulent heat (W)
				max	mean	s.d.	max	mean	s.d.	
	Hindcast	1986	14-18 Dec	–48.8	–18.9	18.5	7,811	4,120	2,822	-3.56×10^{11}
		2011	15-18 Feb	–116	–91.6	21.7	601	322	236	-1.25×10^{11}
		2017	10 Feb	–1.59	–1.59	n/a	172	172	n/a	-2.74×10^{8}
		2018	20 Feb-1 Mar	–124	–60.9	39.4	13,000	4,210	4,390	-2.03×10^{12}
DPLE	1985-initialized ensemble #4	1988	17-21 Jan	–194	–103	79.8	429	309	130	-1.54×10^{11}
	2015-initialized ensemble #2	2024	20-24 Jan	–110	–74.1	23.8	6,090	2,540	2,340	-8.87×10^{11}

Table 3. The polynya events, defined when daily dynamic sea ice removal is greater than 10 km^3/day (i.e., dynamic volume tendency (DVT) ≤ -10 km^3/day) for more than three consecutive days, and the corresponding wind condition near Cape Morris Jessup as well as sea ice thickness (SIT) over northern Greenland from the RASM-DPLE simulation, initialized on December 1st, 1985. A correlation coefficient (r) is calculated between daily DVT and North-South wind for December-March and the bold indicates the largest polynya event.

DPLE ensemble member	Year	Month	No. of days when DVT ≤ -10 km^3/day	Five-day mean SIT (m) before polynya	Daily mean DVT (km^3/day)	Total Ice removal (km^3)	North-South wind during polynya			r ($p<0.01$) between daily DVT and North-South wind (Dec-Mar)
							Time-integrated pseudo–wind stress* (m^2/s^2·day)	Mean speed (m)	Max. speed (m)	
1	1986	Jan	3	4.1	–16.1	–48	307	9.7	13.6	–0.73
1	1986	Mar	4	4.4	–12.6	–50	31	2.5	4.3	–0.73
1	1988	Mar	3	4.0	–11.5	–35	168	7.4	9.9	–0.76
1	1990	Mar	4	3.5	–15.6	–62	395	8.6	15.5	–0.72
1	1991	Dec	3	3.8	–17.6	–53	244	8.6	12.2	–0.66
2	1991	Dec	6	3.8	–22.3	–134	761	10.6	14.7	–0.81
3	1987	Jan	4	3.8	–21.4	–85	475	10.1	19.0	–0.69
4	1986	Dec	6	3.7	–16.9	–101	439	7.6	15.2	–0.78
4	**1988**	**Jan**	**7**	**4.2**	**–17.2**	**–120**	**438**	**7.6**	**12.0**	**–0.64**
4	1989	Feb	5	4.0	–20.7	–104	651	11.2	15.7	–0.70
4	1991	Feb	3	3.2	–25.2	–76	550	12.6	17.8	–0.81
4	1991	Dec	3	3.6	–13.5	–40	230	8.3	12.9	–0.78
5	1986	Jan	4	3.8	–17.0	–68	260	7.3	13.7	–0.70
5	1987	Jan	4	3.5	–16.5	–66	121	4.9	8.5	–0.68
5	1987	Dec	4	3.4	–13.9	–55	438	10.1	14.1	–0.61
5	1988	Mar	3	3.8	–20.0	–60	121	4.8	11.2	–0.61
6	1986	Dec	3	3.4	–12.6	–38	111	5.6	10.0	–0.74
6	1994	Feb	4	2.9	–22.0	–88	700	13.0	16.7	–0.73
7	1990	Dec	3	3.3	–20.8	–62	283	9.4	12.6	–0.73
7	1994	Jan	3	3.8	–14.7	–44	255	8.5	12.3	–0.65
8	1992	Jan	3	4.3	–13.6	–41	277	9.2	15.0	–0.71
8	1995	Jan	3	3.3	–16.9	–51	172	6.9	13.0	–0.63
9	1989	Dec	4	4.0	–13.2	–53	228	7.1	10.9	–0.71
9	1995	Mar	3	3.8	–16.3	–49	322	10.2	11.6	–0.66
10	1987	Feb	3	3.6	–13.2	–40	145	6.6	10.1	–0.62

* only for the northward wind component

730

Table 4. Same as Table 3, but for the RASM–DPLE simulation, initialized on December 1st, 2015.

DPLE ensemble member	Year	Month	No. of days when DVT ≤ –10 km^3/day	Five-day mean SIT (m) before polynya	Daily mean DVT (km^3/day)	Total Ice removal (km^3)	North-South wind during polynya			*r* (p<0.01) between daily DVT and North-South wind (Dec-Mar)
							Time-integrated pseudo–wind stress* (m^2/s^2·day)	Mean speed (m)	Max. speed (m)	
1	2016	Feb	5	2.7	–14.4	–72	165	5.0	10.1	–0.75
1	2022	Feb	3	2.6	–15.1	–45	216	8.2	11.5	–0.62
1	2023	Jan	3	2.5	–14.4	–43	321	10.0	14.3	–0.78
1	2023	Jan	3	1.8	–15.4	–46	299	9.8	13.1	–0.78
2	2016	Jan	3	2.8	–16.4	–49	192	7.8	10.9	–0.76
2	**2024**	**Jan**	**7**	**3.3**	**–19.4**	**–136**	**841**	**9.8**	**19.2**	**–0.78**
4	2019	Mar	3	3.0	–15.4	–46	235	7.4	16.9	–0.63
5	2018	Jan	5	3.0	–20.8	–104	740	10.8	17.9	–0.77
5	2018	Mar	3	3.0	–15.4	–46	129	5.6	12.9	–0.77
5	2020	Feb	5	3.0	–15.5	–77	379	8.4	12.2	–0.75
6	2016	Jan	4	2.8	–12.1	–48	379	9.6	12.3	–0.77
6	2018	Dec	3	3.0	–15.1	–45	358	10.4	16.2	–0.71
6	2024	Jan	4	2.8	–20.0	–80	352	8.1	15.2	–0.72
7	2023	Dec	4	3.4	–16.4	–66	305	8.2	14.8	–0.70
8	2017	Feb	3	2.9	–14.5	–43	558	13.1	17.0	–0.79
8	2025	Jan	5	2.8	–18.5	–92	531	9.9	15.8	–0.76

* only for the northward wind component

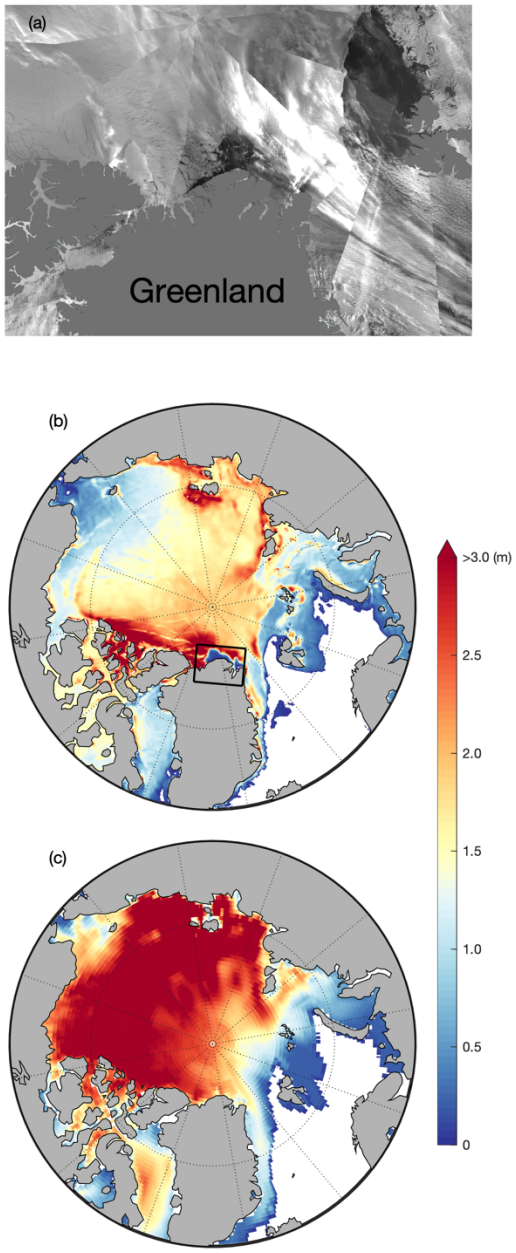

Figure 1: (a) The Visible Infrared Imaging Radiometer Suite (VIIRS) Nighttime Imagery (Day/Night Band, Enhanced Near Constant Contrast) over the northern Greenland on 25 February 2018 (adapted from NASA Worldview at https://worldview.earthdata.nasa.gov) and sea ice thickness from (b) the RASM hindcast simulation as well as (c) CFS version 2 reanalysis over the Arctic on 25 February 2018. The rectangular box indicates the polynya area.

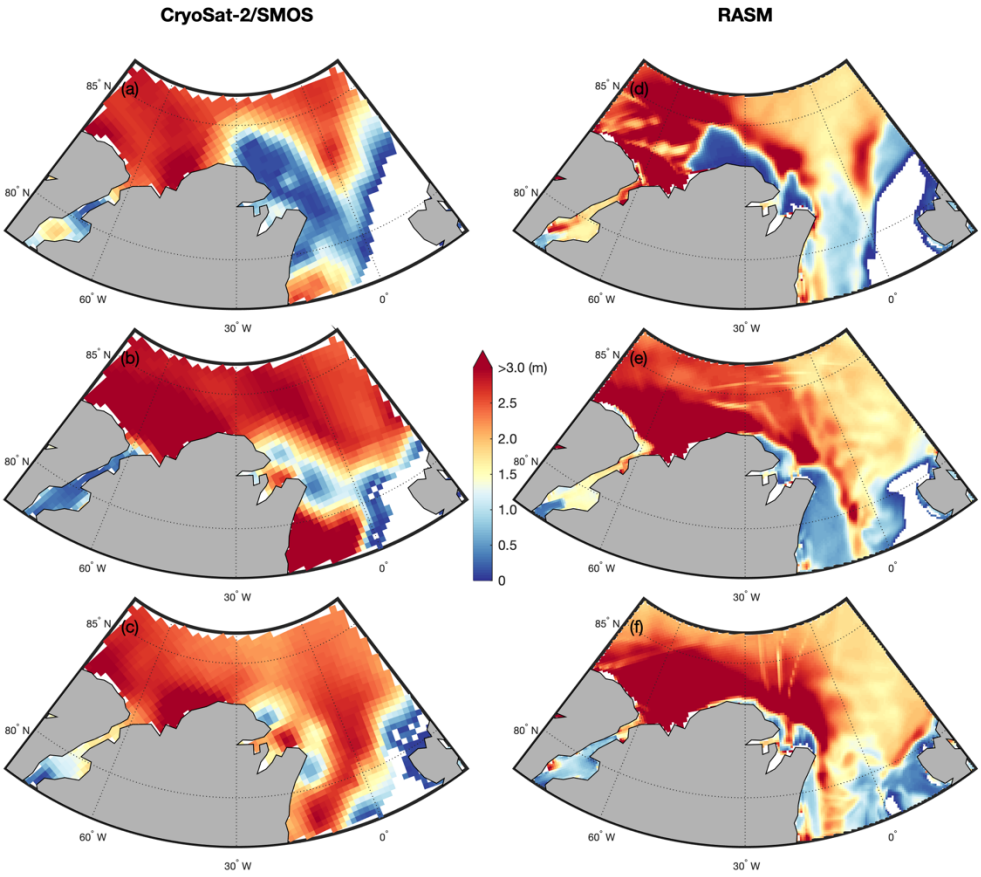

Figure 2: Mean sea ice thickness (SIT) over the northern Greenland region from the CryoSat-2/SMOS merged product on (a) 22-28 February 2018, (b) 8-14 February 2017, and (c) 13-19 February 2011 as well as daily SIT from the RASM hindcast simulation on (d) 25 February 2018, (e) 11 February 2017, and (f) 16 February 2016.

745

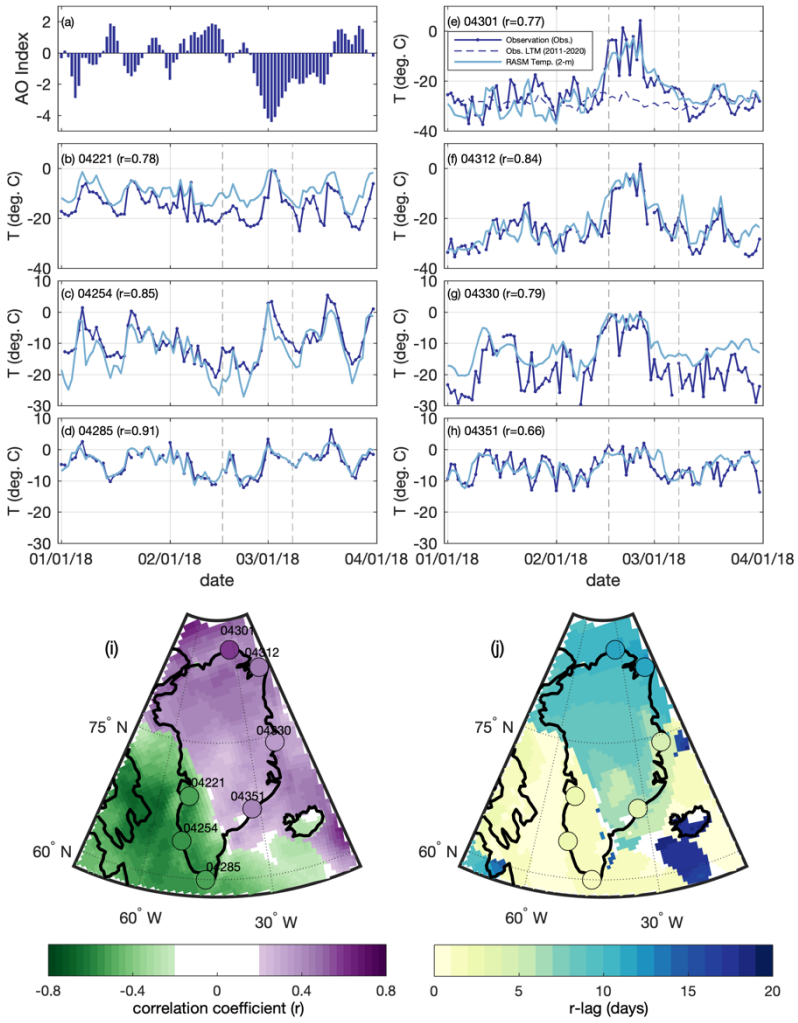

Figure 3. (a) The observed daily AO index and (b)-(h) the daily mean near-surface air temperature (T, ^{o}C; blue) during January-March 2018 from the selected weather stations around Greenland as shown in (i) and (j) as circle markers. The RASM daily 2-m air temperature (light blue) is from the nearest grid cell and the observed long-term daily mean (LTM, 2011-2020; blue-dashed) is only at Station 04301. The correlation coefficient (r) is statistically significant (p<0.05) between the observed and the simulated air temperature is shown in the upper-left. The vertical dashed lines indicate the start and end dates of the 2018 winter polynya period. The spatial maps show (i) the maximum correlation coefficients and (j) their lagged time-scales (days) between the AO index and the RASM air temperature. Note that grid cells not statically significant (p>0.05) are indicted as white. The color-scale of the markers quantifies the relationship between the AO index and the observed air temperature at each weather station.

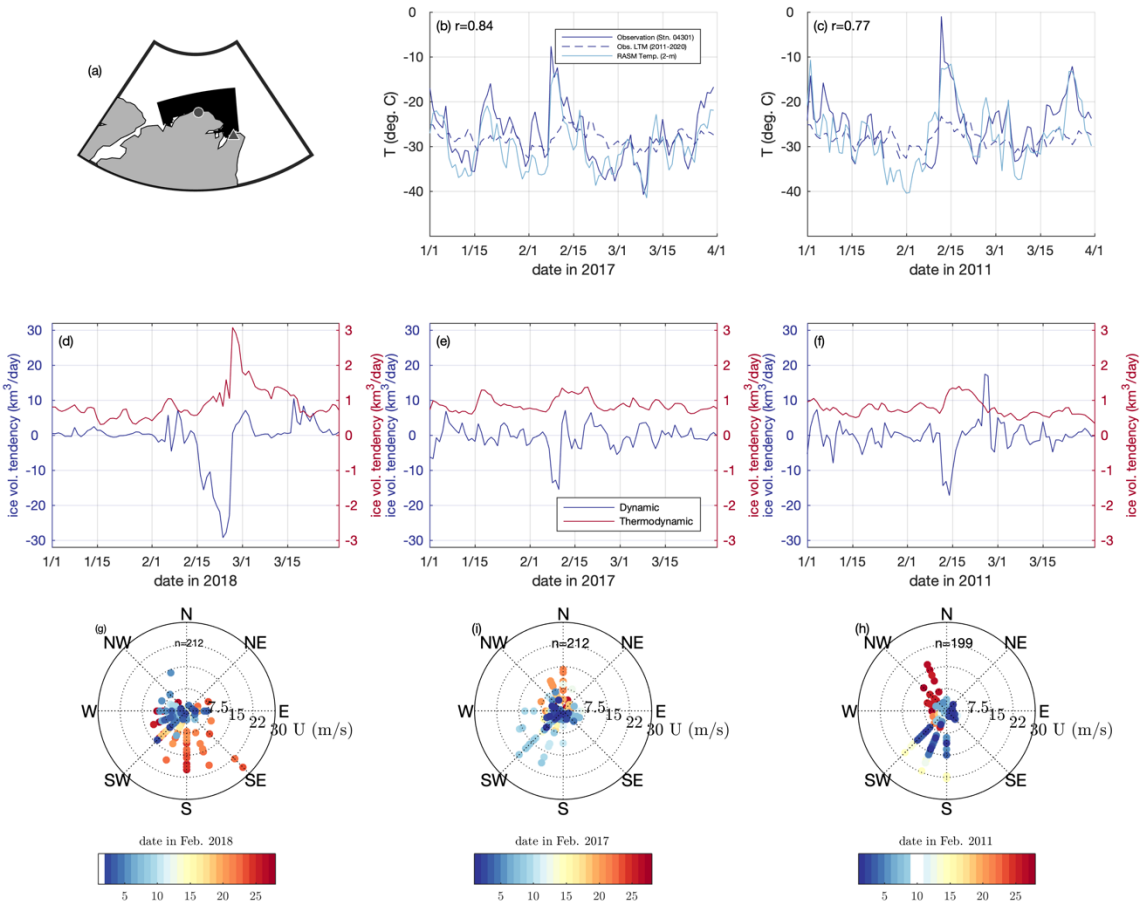

760 **Figure 4. The observed daily near-surface air temperature (T, ^{o}C; blue) from Station 04301 (Cape Morris Jesup as ●) in (a) and the RASM daily 2-m air temperature (light blue) from the nearest grid cell during January-March of (b) 2017 and (c) 2011; the observed long-term daily mean (LTM, 2011-2020; blue-dashed). The correlation coefficient (*r*) between the observed and the simulated air temperature is shown in the upper-left. Time rate of change of the RASM daily sea ice volume (km^3/day) due to thermodynamic (red) and dynamic (blue) tendency during January-March of (d) 2018, (e) 2017, and (f) 2011, spatially integrated**
765 **for the black-shaded area in (a). Wind rose plots of 3-hourly wind data at Station 04312 (Station Nord as ▲) during February of (g) 2018, (h) 2017, and (i) 2011: wind speed (U, m/s) and direction. The missing data are indicted as white in each color bar.**

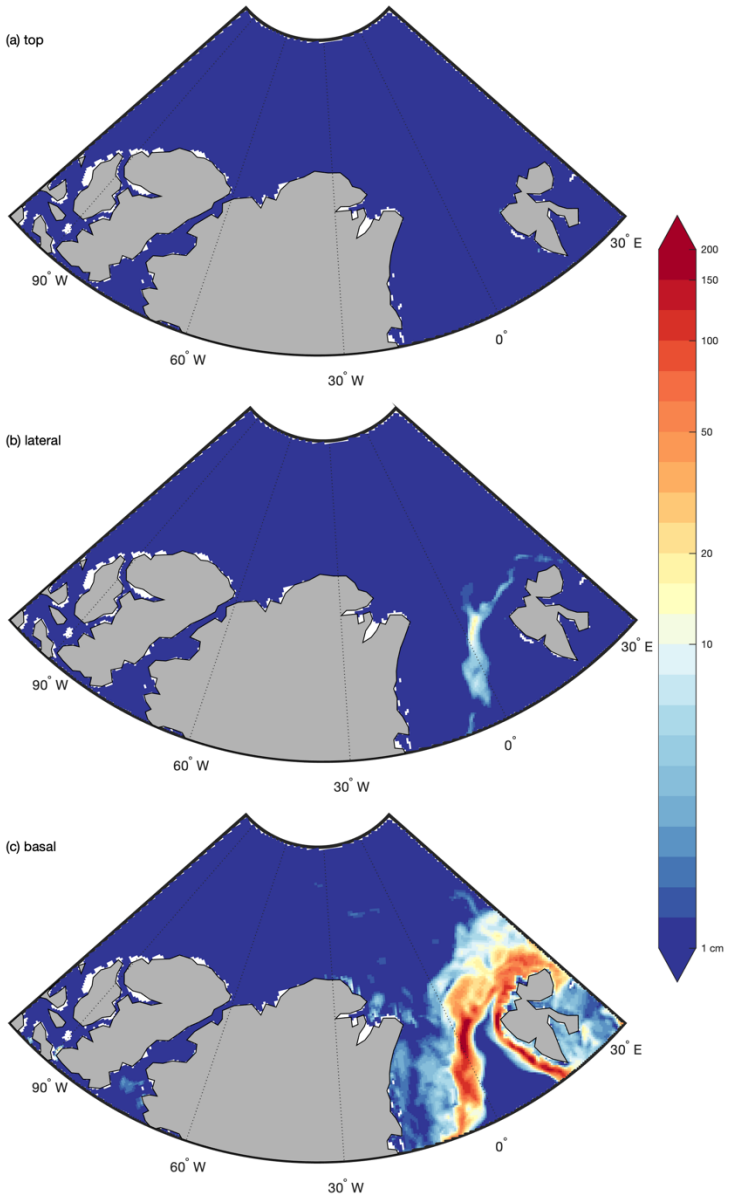

Figure 5. Monthly integrated sea ice melt terms over the northern Greenland region during February 2018 from the RASM hindcast simulation: (a) surface top, (b) lateral, and (c) basal melt (cm).

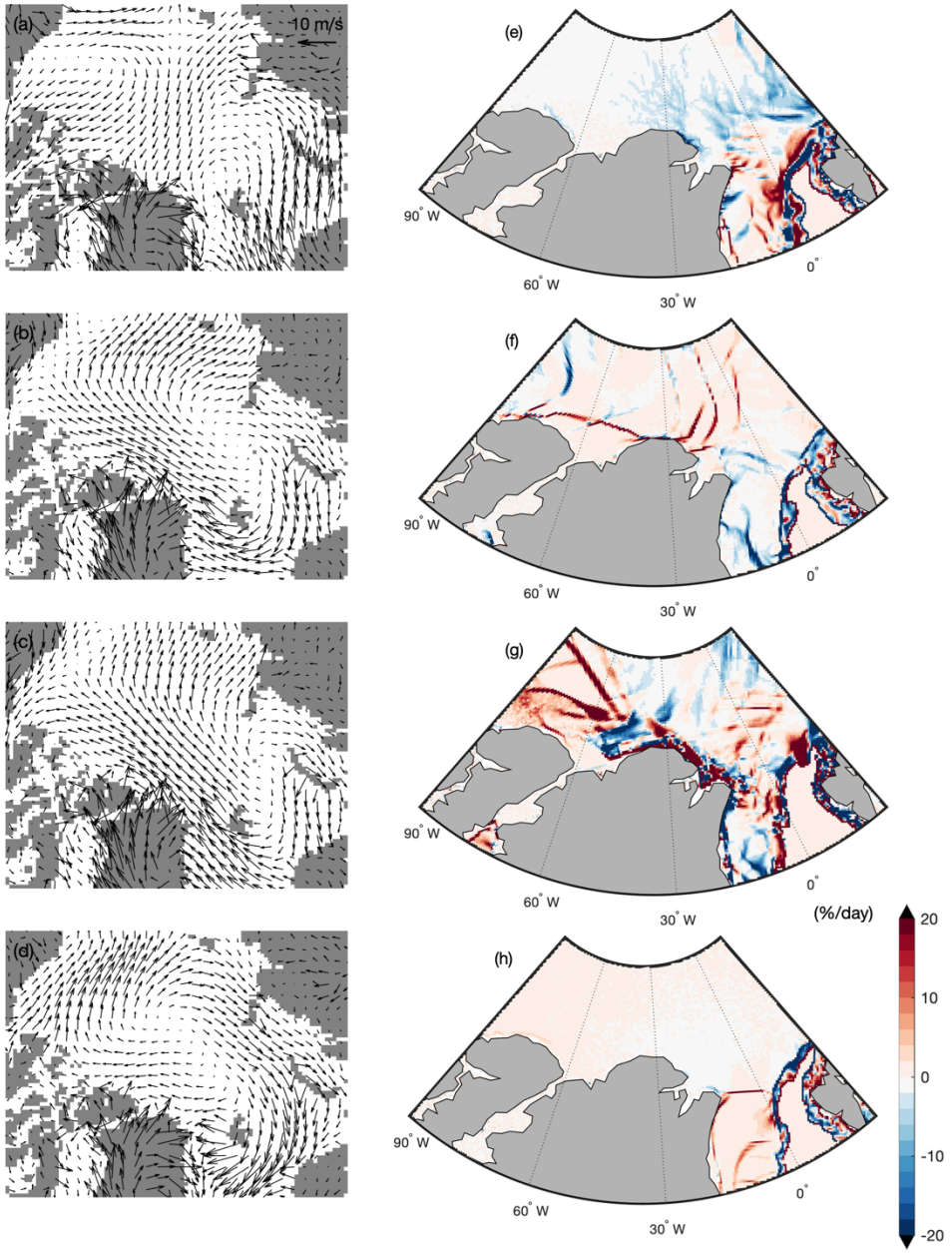

Figure 6. Four major patterns with self-organizing maps (frequency of occurrence as %) of the near-surface 6-hourly wind fields from the RASM simulation during the time periods including before and after the 2018 polynya event: (a) 5-11 February (93%), (b) 15-20 February (83%), (c) 20-26 February (93%), and (d) 3-13 March (95%). The wind vectors were sub-sampled at every 3 grid-cells for a plotting purpose. RASM daily sea ice divergence (%/day) within each period above is shown on (e) 10 February, (f) 16 February, (g) 24 February, and (h) 4 March 2018.

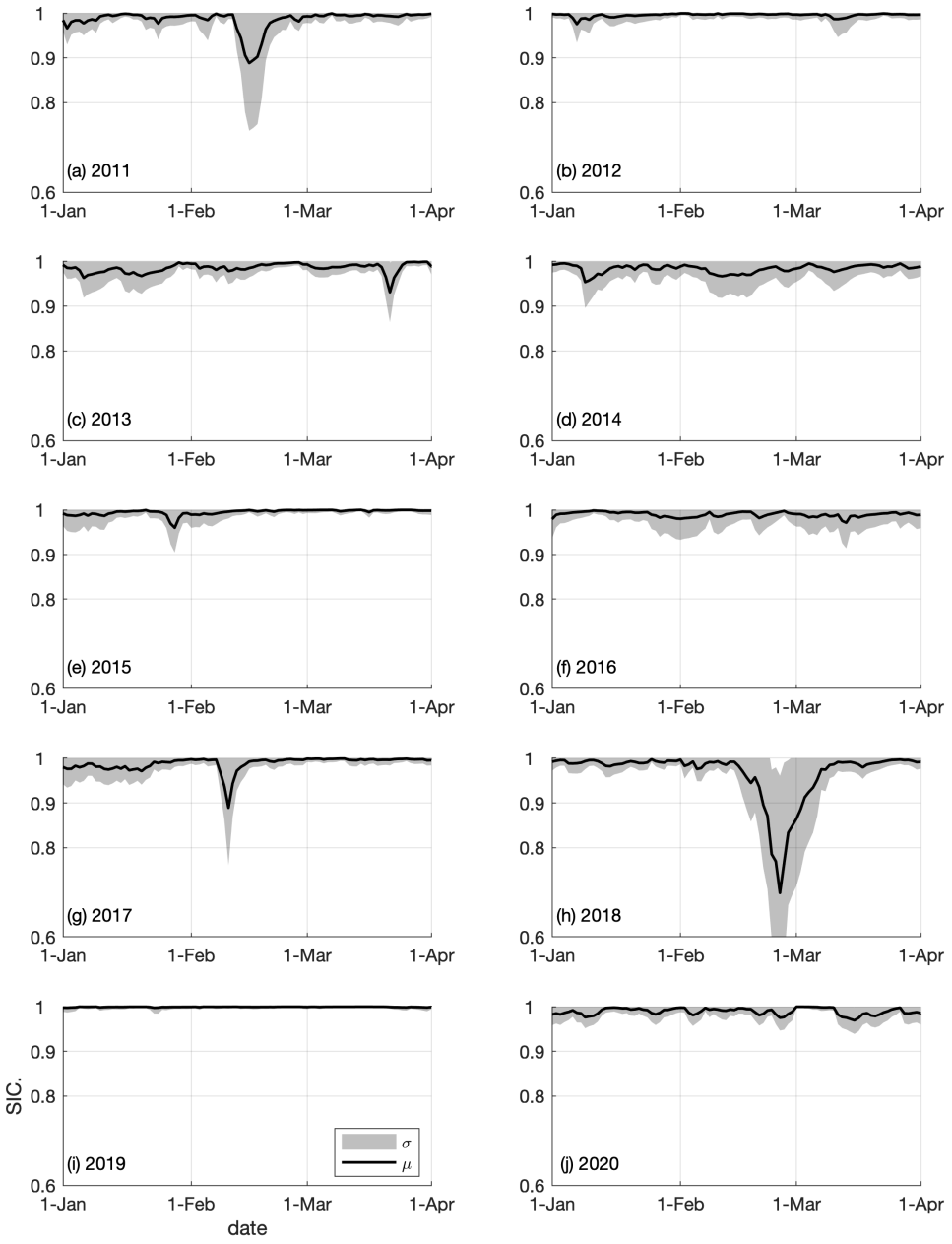

Figure 7. (a)-(j) Satellite-derived (NASA team algorithm) daily mean sea ice concentration (SIC, μ; black) for the northern Greenland region (see Fig. 4a) during January-March from 2011 to 2020. The grey shading depicts one standard deviation (σ; gray) from the mean.

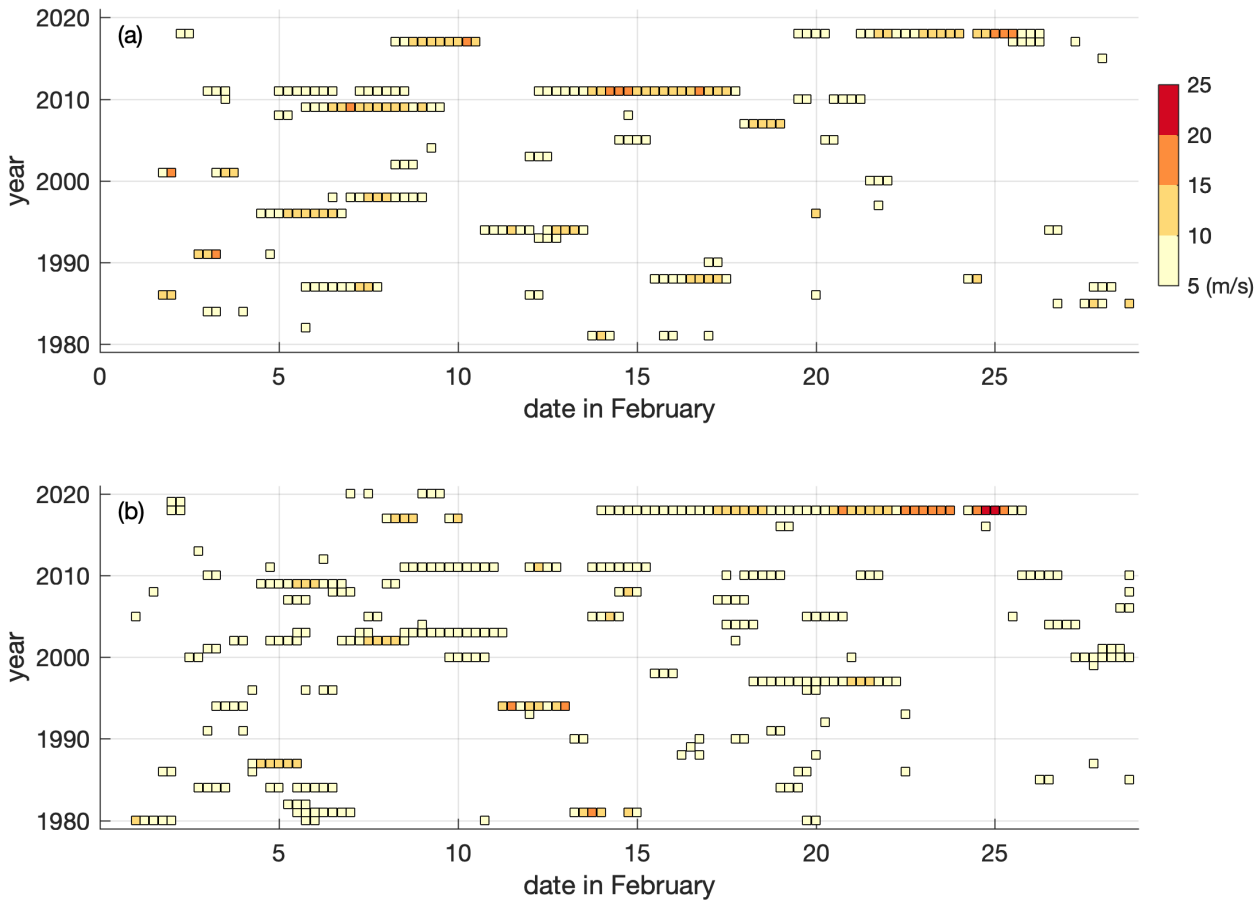

Figure 8. The northward wind component greater than 5 m/s from the RASM hindcast simulation during February of 1980-2020 at the nearest grid to (a) Station 04312 (Station Nord) and (b) Station 04301 (Cape Morris Jesup). Each square represents the six-hourly surface wind and its color indicates a magnitude of wind speed.

785

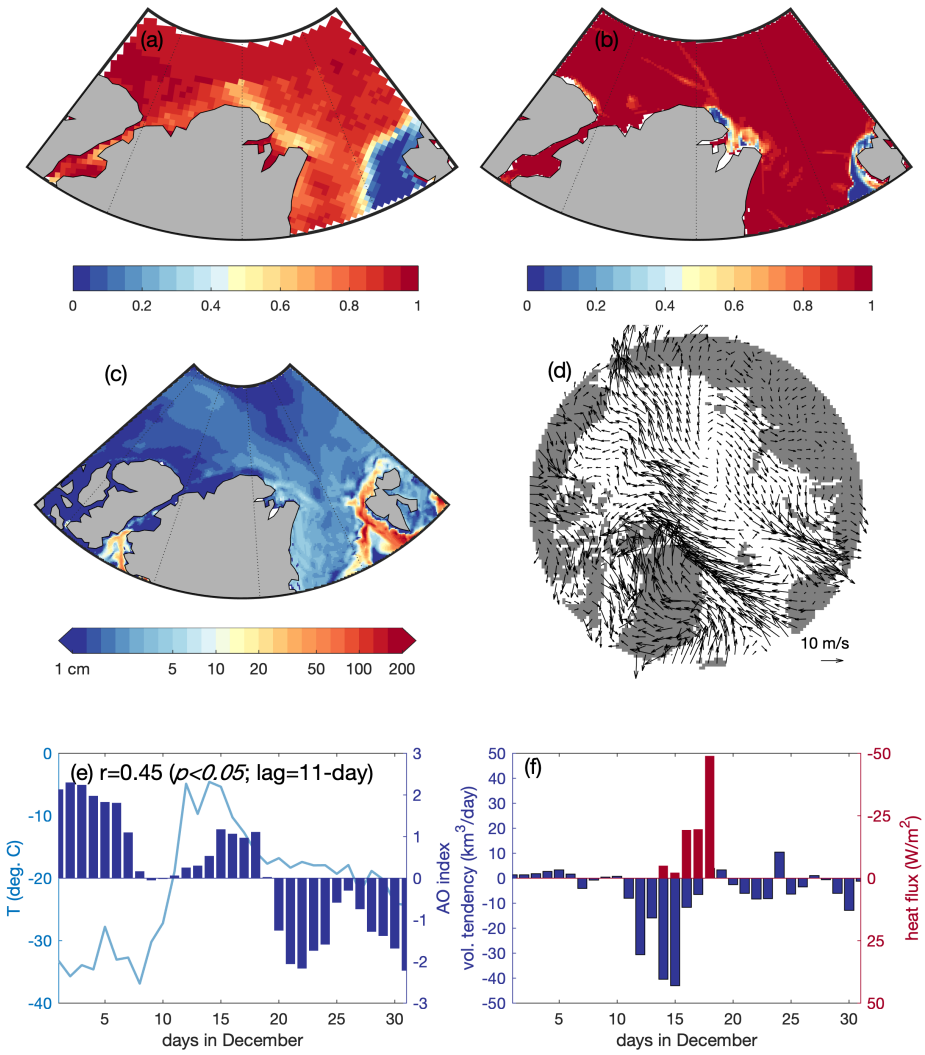

Figure 9. Mean sea ice concentration (NASA Team algorithm) on 15 December 1986 over the northern Greenland region from (a) the Nimbus-7 SMMR and (b) the RASM hindcast simulation. (c) Monthly integrated sea ice melt (top, lateral, and basal) for December 1986 and (d) near-surface (at 10 m) wind fields on 12 December 1986 from the RASM hindcast simulation. (e) RASM daily near-surface air temperature (ligh blue) from the nearest grid cell to Station 04301 (Cape Morris Jesup) and daily AO index (blue) in December 1986. The correlation coefficient (r) between theAO index and the simulated air temperature is shown in the upper-left. (f) Time rate of change of the RASM daily sea ice volume (km^3/day; blue) due to dynamic tendency during December 1986, spatially integrated for the region shown in Fig. 4a. Daily mean net turbulent (sensible and latent) heat flux (W/m^2; red) is also shown over the same region where sea ice thickness is less than 10 cm from the RASM hindcast simulations. The negative values indicate loss from the region.

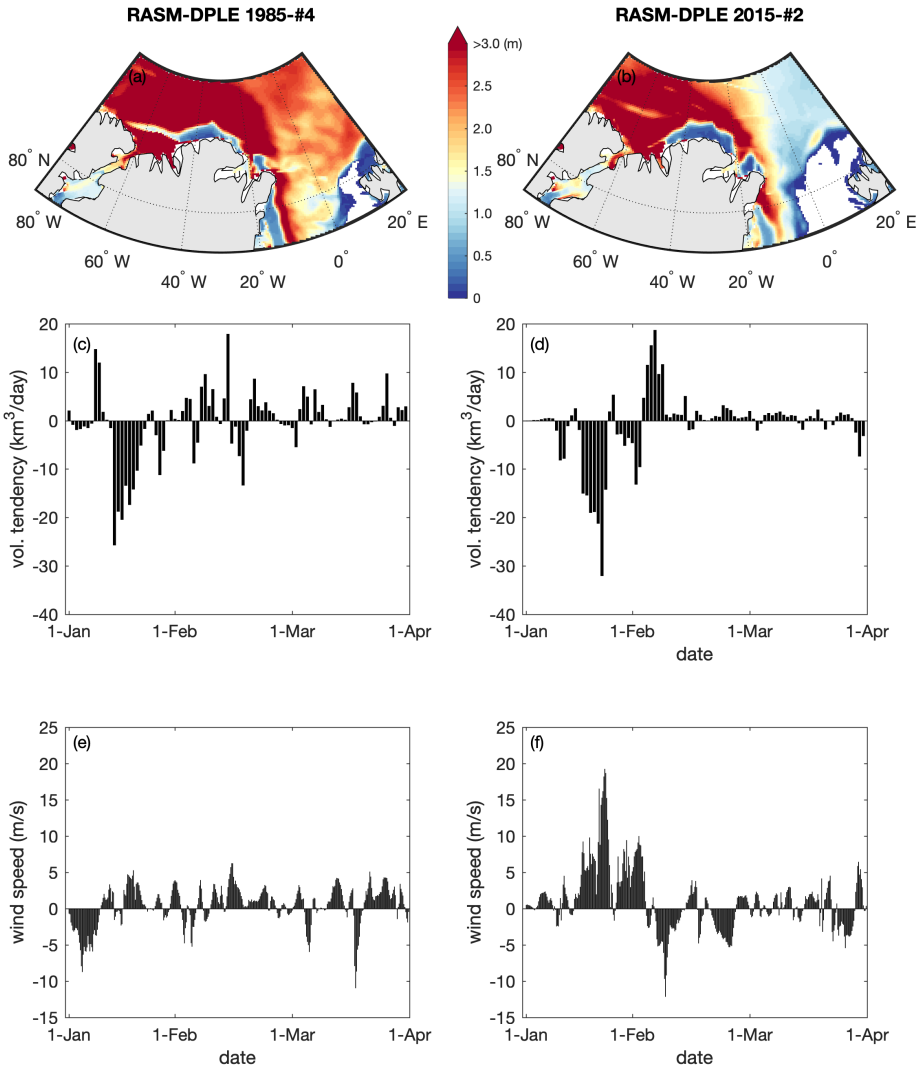

Figure 10. Sea ice thickness (SIT, m), sea ice dynamic volume tendency (DVT, km^3/day) for the northern Greenland region (see Fig. 4a), and north(positive)-south(negative) wind component (m/s) during winter months from the ensemble member #4 in the 1985-initialized run and the ensemble member #2 in the 2015-initialized run: SIT on (a) 22 January 1988 and (b) 14 January 2024, daily DVT in January-March of (c) 1988 and (d) 2024, and six-hourly north-south wind in January-March of (e) 1998 and (f) 2024.